Structure
Ways & Means

Genetic Encoding of 3-Iodo-L-Tyrosine in *Escherichia coli* for Single-Wavelength Anomalous Dispersion Phasing in Protein Crystallography

Kensaku Sakamoto,[1,6] Kazutaka Murayama,[1,2,6] Kenji Oki,[1,3] Fumie Iraha,[1] Miyuki Kato-Murayama,[1] Masahiro Takahashi,[3,7] Kazumasa Ohtake,[1,3] Takatsugu Kobayashi,[1,3] Seiki Kuramitsu,[4,5] Mikako Shirouzu,[1] and Shigeyuki Yokoyama[1,3,*]

[1]RIKEN Systems and Structural Biology Center, 1-7-22 Suehiro-cho, Tsurumi, Yokohama 230-0045, Japan
[2]Division of Biomedical Measurements and Diagnostics, Graduate School of Biomedical Engineering, Tohoku University, 2-1 Seiryo-machi, Aoba, Sendai 980-8575, Japan
[3]Department of Biophysics and Biochemistry, Graduate School of Science, The University of Tokyo, 7-3-1 Hongo, Bunkyo-ku, Tokyo 113-0033, Japan
[4]RIKEN SPring-8 Center, Harima Institute, 1-1-1 Kouto, Sayo, Hyogo 679-5148, Japan
[5]Department of Biological Sciences, Graduate School of Science, Osaka University, Osaka 560-0043, Japan
[6]These authors contributed equally to this work.
[7]Present address: Laboratories of Nanobiology, Graduate School of Frontier Biosciences, Osaka University, 1-3 Yamadaoka, Suita, Osaka, 565-0871, Japan.
*Correspondence: yokoyama@biochem.s.u-tokyo.ac.jp
DOI 10.1016/j.str.2009.01.008

SUMMARY

We developed an *Escherichia coli* cell-based system to generate proteins containing 3-iodo-L-tyrosine at desired sites, and we used this system for structure determination by single-wavelength anomalous dispersion (SAD) phasing with the strong iodine signal. Tyrosyl-tRNA synthetase from *Methanocaldococcus jannaschii* was engineered to specifically recognize 3-iodo-L-tyrosine. The 1.7 Å crystal structure of the engineered variant, iodoTyrRS-*mj*, bound with 3-iodo-L-tyrosine revealed the structural basis underlying the strict specificity for this nonnatural substrate; the iodine moiety makes van der Waals contacts with 5 residues at the binding pocket. *E. coli* cells expressing iodoTyrRS-*mj* and the suppressor tRNA were used to incorporate 3-iodo-L-tyrosine site specifically into the ribosomal protein *N*-acetyltransferase from *Thermus thermophilus*. The crystal structure of this enzyme with iodotyrosine was determined at 1.8 and 2.2 Å resolutions by SAD phasing at CuKα and CrKα wavelengths, respectively. The native structure, determined by molecular replacement, revealed no significant structural distortion caused by iodotyrosine incorporation.

INTRODUCTION

The site-specific incorporation of ''nonnatural'' amino acids into proteins is a useful tool to introduce unique chemical groups, which are not found among the 20 canonical amino acids, into proteins at desired sites. Nonnatural amino acids have been incorporated into proteins not only by using cell-free translation systems (Noren et al., 1989; Bain et al., 1989; Cornish et al., 1995; Hohsaka et al., 2001), but also in living cells, such as *Escherichia coli* (Wang et al., 2001), yeast (Chin et al., 2003), and mammalian cells (Sakamoto et al., 2002; Ye et al., 2008). These cell-based systems facilitate the preparation of proteins containing nonnatural amino acids or ''alloproteins'' in sufficient amounts for structural and biochemical studies.

A cell-based system relies on the expression of the exogenous pair of a suppressor tRNA and an aminoacyl-tRNA synthetase (aaRS) variant, which is engineered to specifically recognize a nonnatural amino acid as its substrate. In *E. coli*, the pair of an amber suppressor tRNA and a variant of tyrosyl-tRNA synthetase from *Methanocaldococcus jannaschii* has been expressed to translate amber codons into nonnatural amino acids (Wang et al., 2001). This tRNA•aaRS pair does not crossreact with any endogenous tRNA and aaRS species from *E. coli*, which guarantees that only nonnatural amino acids are incorporated at the amber positions, and that these amino acids are not incorporated at other positions.

This cell-based production of alloproteins containing iodine atoms can be applied to protein crystallography. The phasing method utilizing multiwavelength anomalous diffraction of synchrotron radiation by selenium has been a mainstream method and has accelerated the determination of protein structures (Hendrickson, 1991). Single-wavelength anomalous dispersion (SAD) with sulfur, which is observable on in-house X-ray sources, has also been utilized in the structure determinations (Teeter and Hendrickson, 1979; Li et al., 2008). The intensity of the anomalous signal of iodine is 12- and 11-fold larger than that of the signal of sulfur at the CuKα and CrKα wavelengths, respectively (Dauter et al., 2002), both of which are available on in-house X-ray generators. Due to these advantages, the incorporation of iodine atoms into proteins seems promising, when it is employed together with SAD phasing. Although proteins can be iodinated on tyrosine residues with

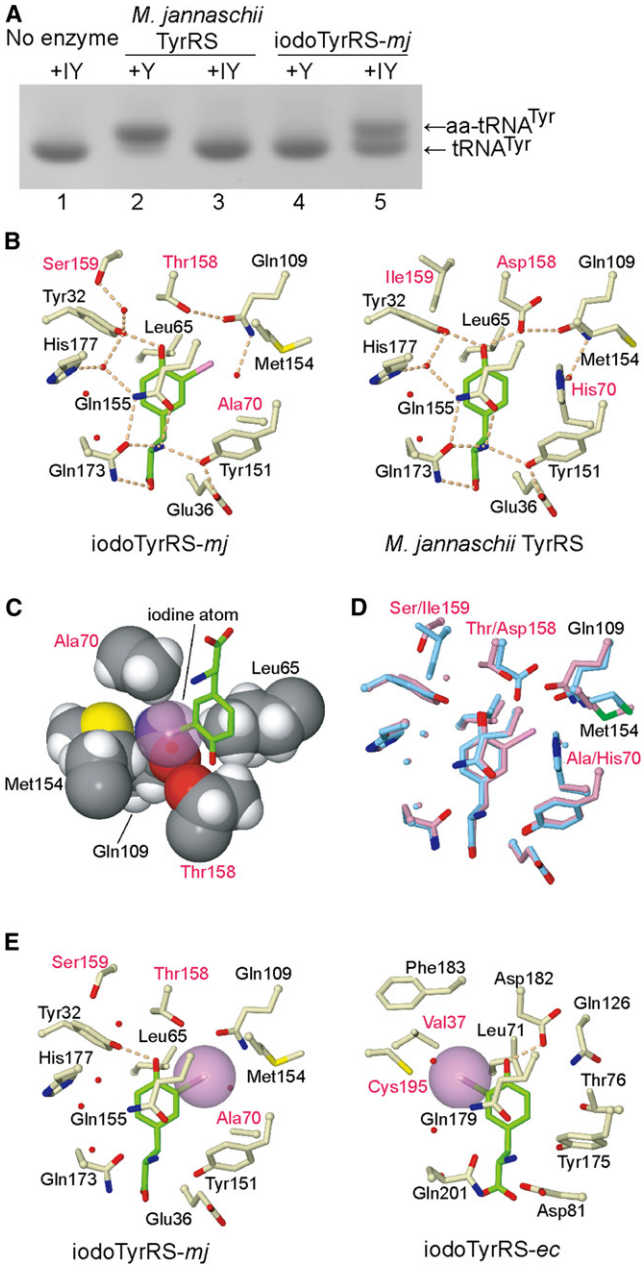

Figure 1. Engineering of IodoTyrRS-*mj* and the Structural Basis Underlying Its Specificity for 3-Iodo-L-Tyrosine

(A) The amino acid specificity of iodoTyrRS-*mj* was analyzed by acidic polyacrylamide gel electrophoresis of $tRNA^{Tyr}$ molecules subjected to aminoacylation with 3-iodo-L-tyrosine (+IY) and L-tyrosine (+Y), in the presence of no enzyme, *M. jannaschii* TyrRS, and iodoTyrRS-*mj*. The bands corresponding to *M. jannaschii* $tRNA^{Tyr}$ ($tRNA^{Tyr}$) and the aminoacylated $tRNA^{Tyr}$ (aa-$tRNA^{Tyr}$) are indicated.

(B) The amino acid-binding pocket in the crystal structure of iodoTyrRS-*mj*, complexed with 3-iodo-L-tyrosine (left), is compared with the L-tyrosine-bound pocket of *M. jannaschii* TyrRS (Kobayashi et al., 2003) (right). The carbon and iodine atoms of the substrate are depicted by green and pink sticks, respectively. Water oxygens are represented by red spheres. Hydrogen bonding is indicated by a dotted line. The mutated residues and the corresponding wild-type residues are denoted in red.

(C) The van der Waals contacts between the iodine atom of the bound 3-iodo-L-tyrosine and the 5 residues of iodoTyrRS-*mj* shown in the Corey-Pauling-Koltun model. The iodine atom is shown by a purple sphere.

(D) Superposed amino acid-binding pockets of iodoTyrS-*mj* (pink) and *M. jannaschii* TyrRS (blue).

(E) The 3-iodo-L-tyrosine-bound pocket of iodoTyrRS-*mj* (left) is compared with the corresponding pocket of iodoTyrRS-*ec* (Kobayashi et al., 2005a) (right). Only the hydrogen bonding for the phenolic hydroxyl group is indicated. The van der Waals radius of the iodine atom is shown by a purple sphere.

chemical reagents, this approach causes heterogeneity among the iodinated proteins, with regard to the iodine atom occupancy at each tyrosine position. The site-specific incorporation of an iodinated amino acid should achieve nearly full occupancy of the iodine atoms at desired sites.

The feasibility of the latter approach has been demonstrated by using a model system of bacteriophage T4 lysozyme and 4-iodo-L-phenylalanine (Xie et al., 2004). A lysozyme variant with a particular Phe residue replaced by iodophenylalanine formed crystals that led to successful SAD phasing at the CuKα wavelength. However, the incorporation of iodinated amino acids raises the general concern about fatal steric hindrance, possibly caused by the bulky iodine atom. It is preferable to replace the residues near the surface of a protein by iodinated amino acids. Phe is found buried in proteins as frequently as it is found exposed to the solvent, but Tyr generally tends to be solvent exposed (Bordo and Argos, 1991).

In the present study, to enable the use of an iodinated tyrosine derivative, we developed an *Escherichia coli* cell-based system for site specifically incorporating 3-iodo-L-tyrosine into proteins. *M. jannaschii* TyrRS was engineered to create a highly specific variant (iodoTyrRS-*mj*) for this nonnatural amino acid. This system was utilized to determine the crystal structure of the ribosomal protein *N*-acetyltransferase, the product of the *rimL* gene (Henne et al., 2004), from *Thermus thermophilus*.

RESULTS

Isolation of an *M. jannaschii* TyrRS Variant Specific to 3-Iodo-L-Tyrosine

In the crystal structure of the ternary complex of *M. jannaschii* TyrRS•$tRNA^{Tyr}$•L-tyrosine (Kobayashi et al., 2003), Tyr32, His70, Asp158, and His177 are located in the proximity of position 3 of the phenolic ring of L-tyrosine (the structure of the binding pocket of *M. jannaschii* TyrRS is shown in Figure 1B). Since His70 and His177 are located near the opposite sides of the phenolic ring, we constructed two different libraries of *M. jannaschii* TyrRS variants. In one library, Tyr32, His70, and Asp158 were randomly replaced by the other amino acids, whereas Tyr32, Asp158, and His177 were replaced in the other library. In addition, Asp286 was replaced by Tyr in each variant, to enhance the recognition of the amber suppressor tRNA (Kobayashi et al., 2003).

These libraries were expressed in *E. coli* cells, together with the *M. jannaschii* amber suppressor tRNA and an amber mutant gene encoding chloramphenicol acetyltransferase (CAT). The ability of each variant to selectively esterify 3-iodo-L-tyrosine to the tRNA was examined in terms of the amber suppression conferring resistance to Cm, in the presence of 3-iodo-L-tyrosine

supplemented in the growth media. A variant with the double substitution of His70Ala and Asp158Thr was thus found to confer resistance to chloramphenicol (Cm) at a concentration of 50 μg/ml, only in the presence of 3-iodo-L-tyrosine. We then introduced additional replacements into this variant at random positions, and we discovered that another substitution, Ile159Ser, increased the resistance to Cm up to a concentration of 200 μg/ml. Cells expressing this variant, TyrRS(H70A-D158T-I159S-D286Y) or iodoTyrRS-*mj*, are still sensitive to Cm at 50 μg/ml in the absence of 3-iodo-L-tyrosine, showing that the enzyme doe not esterify any endogenous amino acid in the cell to the suppressor tRNA.

To characterize its in vitro activity, iodoTyrRS-*mj* was prepared from an overproducing *E. coli* strain. *M. jannaschii* $tRNA^{Tyr}$ was then subjected to aminoacylation by *M. jannaschii* TyrRS and iodoTyrRS-*mj*, in the presence of L-tyrosine or 3-iodo-L-tyrosine. Aminoacylated and uncharged tRNA molecules can be separated by acidic polyacrylamide gel electrophoresis (PAGE) (Varshney et al., 1991). With no enzyme added, 3-iodo-L-tyrosine did not affect the mobility of uncharged tRNA on the gel (Figure 1A, lane 1). The addition of *M. jannaschii* TyrRS to the reaction changed the mobility only in the presence of L-tyrosine (lanes 2 and 3), showing that the enzyme esterified L-tyrosine, but not 3-iodo-L-tyrosine, to $tRNA^{Tyr}$. In contrast, iodoTyrRS-*mj* esterified 3-iodo-L-tyrosine, but not L-tyrosine, to $tRNA^{Tyr}$ (lanes 4 and 5). A fraction of $tRNA^{Tyr}$ remained uncharged with 3-iodo-L-tyrosine, because the D286Y mutation in iodoTyrRS-*mj* reduces the activity for $tRNA^{Tyr}$ by six-fold (Kobayashi et al., 2003). In addition, the activity of this variant with 3-iodo-L-tyrosine is probably lower than that of *M. jannaschii* TyrRS with L-tyrosine. The result of this in vitro assay showed that the specificity of iodoTyrRS-*mj* has clearly been converted from L-tyrosine to 3-iodo-L-tyrosine.

Mass spectrometric analyses were performed to confirm the identity of the amino acid incorporated at the amber position by iodoTyrRS-*mj*. A mutant glutathione *S*-transferase (GST) gene, with an amber codon at position 25, was expressed together with iodoTyrRS-*mj* and the suppressor tRNA in the presence of 3-iodo-L-tyrosine. As a control sample, GST containing Tyr at position 25 was also prepared. After trypsin digestion, GST(Tyr25) generated a peptide (the Tyr25 peptide) with an average mass corresponding to the theoretical value (m/z = 1327.7) for residues 23–33, NSYSPILGYWK (Tyr25 is underlined) (see Figure S1 available online). The identical peptide was not found from the product of the *gst*(Am25) gene. Instead, we detected a peptide with an average mass (1453.6) larger than that of the Tyr25 peptide by a value (125.9) corresponding to the mass of an iodine atom, less the mass of a hydrogen atom. This result indicated the incorporation of 3-iodo-L-tyrosine at the amber position.

Structural Basis for Specific 3-Iodo-L-Tyrosine Recognition by IodoTyrRS-*mj*

To elucidate the structural basis for the enzyme's strict specificity for 3-iodo-L-tyrosine over L-tyrosine, the crystal structure of iodoTyrRS-*mj* complexed with 3-iodo-L-tyrosine was determined and refined to a final R factor of 19.5% at 1.7 Å resolution (Table 1). The whole structure superposes well on the reported structure of *M. jannaschii* TyrRS in the ternary complex with $tRNA^{Tyr}$ and L-tyrosine, with a root-mean-square deviation (rmsd) of 0.49 Å for the Cα atoms. The L-tyrosine-binding pocket of iodoTyrRS-*mj* is reshaped to fit this nonnatural amino acid, whereas the hydrogen-bonding scheme, involving the recognition of the α-amino and carboxyl groups of L-tyrosine/3-iodo-L-tyrosine, is similar between *M. jannaschii* TyrRS and iodoTyrRS-*mj* (Figure 1B).

The substitutions of His70Ala and Asp158Thr, which were isolated in the first selection, create a space for the bulky iodine moiety of 3-iodo-L-tyrosine and remove the hydrogen bond between the wild-type Asp158 and the phenolic hydroxyl group of L-tyrosine (Figure 1B). The iodine moiety of the substrate makes multiple van der Waals contacts with the δ-methyl group of Leu65, the β-methyl group of Ala70, the γ-carbonyl group of Gln109, the γ-methylene group of Met154, and the β-hydroxyl group of Thr158 (Figure 1C). Among these 5 residues, 3 residues (Leu65, Gln109, and Met154) are not mutated in the variant. The hydrogen bond between Gln109 and Thr158 rigidly fixes their side chains in the proper orientation to contact the iodine atom. Met154 contacts the iodine atom by changing the conformation of its side chain from that found in the wild-type structure (Figure 1D). This conformational change may be induced by the binding of 3-iodo-L-tyrosine to the pocket.

The Ile159Ser substitution was isolated in the second selection, as an enhancer of the activity for 3-iodo-L-tyrosine. This substitution expands the network of hydrogen bonds comprising Tyr32, Gln155, His177, and a water molecule to additionally include Ser159 and another water molecule (Figure 1B). This expanded network rigidly fixes the orientation of the sp^3 lobes of the oxygen atom in the hydroxyl group of Tyr32, probably facilitating the hydrogen bonding between the phenolic hydroxyl groups of Tyr32 and 3-iodo-L-tyrosine.

Application of 3-Iodo-L-Tyrosine in the Structure Determination of the Ribosomal-Protein *N*-Acetyltransferase from *T. thermophilus*

The *E. coli* cell-based system for site specifically incorporating 3-iodo-L-tyrosine into proteins was utilized for the structure determination of the ribosomal protein *N*-acetyltransferase RimL from *T. thermophilus*. This protein has five tyrosines at positions 30, 35, 111, 169, and 188. Since it is difficult to detect amber suppression at position 188 near the C terminus, in terms of the product size, only the four other tyrosine positions were tested for the replacement with iodotyrosine. These positions were individually mutagenized into amber codons, and the generated amber mutants were expressed in *E. coli* cells expressing iodoTyrRS-*mj* and the suppressor tRNA in the presence of 3-iodo-L-tyrosine. The C-terminal Pro194 was removed from each amber variant, to suppress degradation of the variant in *E. coli* cells. The full-length product was expressed from *rimL*(Am30), *rimL*(Am35), and *rimL*(Am111), but not from *rimL*(Am169) (Figure 2A). No full-length product was expressed in the absence of 3-iodo-L-tyrosine. The yields of the full-length variants were 4–5 mg/l LB medium after purification.

RimL(iodoTyr35) and RimL(iodoTyr111) produced crystals under different conditions, whereas no crystal was obtained for RimL(iodoTyr30). An ultracentrifugation analysis indicated that the RimL(iodoTyr30) variant formed aggregates in solution (data not shown). The crystal structure of RimL(iodoTyr111)

Table 1. Data Collection and Refinement Statistics

	IodoTyrRS-*mj*	RimL (IodoTyr111) (*CrKα*)	RimL (IodoTyr111) (*CuKα*)	RimL (Native) (*CuKα*)	RimL (IodoTyr35) (*CuKα*)
Data Collection[a]					
Space group	$P4_32_12$	$P3_221$	$P3_221$	$P3_221$	I4
Cell dimensions					
a, b, c (Å)	102.20, 102.20, 71.90	70.96, 70.96, 99.09	71.40, 71.40, 99.26	71.47, 71.47, 99.16	178.8, 178.8, 122.1
α, β, γ (°)	90, 90, 90	90, 90, 120	90, 90, 120	90, 90, 120	90, 90, 90
Resolution (Å)	50–1.7 (1.76–1.70)	50–2.15 (2.23–2.15)	50–1.77 (1.83–1.77)	50–2.0 (2.07–2.0)	50–2.3 (2.38–2.30)
R_{sym}[b]	0.064 (0.734)	0.076 (0.262)	0.042 (0.266)	0.038 (0.216)	0.089 (0.296)
I/σI	43.4 (2.8)	35.0 (9.6)	34.3 (8.9)	39.1 (8.1)	28.7 (8.5)
Completeness (%)	99.9 (99.9)	99.8 (98.4)	98.9 (90.8)	96.8 (73.6)	97.8 (82.3)
Redundancy	13.7 (11.9)	17.6 (10.3)	9.7 (9.3)	6.4 (2.6)	14.5 (10.7)
Refinement					
Resolution (Å)	41.7–1.7	33.4–2.15	30.9–1.77	31.0–2.0	30.1–2.30
Number of reflections	42,504	16,175	28,933	19,707	42,723
R_{work}/R_{free}[c]	19.3/22.0	20.4/23.2	20.6/23.7	17.0/19.1	22.8/26.6
Number of atoms					
Protein	2474	1535	1535	1569	6144
Ligand	14	–	–	–	–
Water	280	122	184	333	176
B factors					
Protein	31.7	31.6	28.7	18.6	39.2
Ligand/ion	22.2	–	–	43.0	–
Water	44.8	40.0	39.3	33.1	28.4
Rmsds					
Bond lengths (Å)	0.009	0.017	0.013	0.011	0.003
Bond angles (°)	1.50	1.8	1.6	1.5	0.7

[a] Values in parentheses are for the highest-resolution shell.
[b] $R_{sym} = \Sigma\ |I_{avg} - Ii|/\Sigma Ii$, where Ii is the observed intensity, and I_{avg} is the average intensity.
[c] R_{free} is calculated for 10% of randomly selected reflections excluded from refinement.

(Figure 2B) was solved by SAD experiments by using the CuKα and CrKα wavelengths on an in-house X-ray generator, with mean FOM (figure of merit) values of 0.44 (Cu) and 0.54 (Cr) after density modification. Refinement was performed to a final R factor of 20.6% at 1.8 Å resolution and a final R factor of 20.4% at 2.2 Å resolution for the CuKα and CrKα data sets, respectively (Table 1). The RimL(iodoTyr35) crystals were twinned, and its tertiary structure was determined by molecular replacement and refined at 2.3 Å resolution; refinement statistics are provided in Table 1. Although the asymmetric units contain one and four molecules for RimL(iodoTyr111) and RimL (iodoTyr35), respectively, ultracentrifugation analyses indicated that each of these molecules forms a dimer in solution (data not shown). The 2.0 Å crystal structure of the native RimL was also determined by molecular replacement; statistics are provided in Table 1. The rmsd between the native RimL and RimL (iodoTyr111) is 0.25 Å, whereas the rmsd values between the native structure and each of the four RimL(iodoTyr35) structures are 0.88, 0.98, 1.05, and 1.17 Å, respectively.

In the crystal structure of RimL(iodoTyr111), the iodine moiety of iodoTyr111, located in an α helix, protrudes into the solvent (Figure 2C) and electrostatically interacts with the $N_{η2}$ of the guanidino group of Arg115 (Figures 2D and 2E). This guanidino group slightly shifts from its position in the native structure, to accommodate the bulky iodine atom. The phenolic hydroxyl group of Tyr111 hydrogen bonds with the carboxyl group of Glu184 in the native RimL, and this bond is also formed in the variant. In the RimL(iodoTyr35) structure, the iodotyrosine residue is located in the loop connecting the α1 and α2 helices, causing a shift of the main chain around residues 39 and 40 in this loop (Figure S2). The C-terminal residues (189–193) are disordered in both the RimL(iodoTyr35) and RimL(iodoTyr111) structures, whereas all of the residues (1–194) are ordered in the native structure. This disorder is probably due to the removal of Pro194 from the variants, which was retained in the native protein. Thus, no significant structural distortion was caused by the incorporation of iodotyrosine at position 111, whereas the incorporation at position 35 only caused a local structural change in the loop, and did not affect the structure of any other part.

DISCUSSION

Structural Basis for the Strict Amino Acid Specificity of IodoTyrRS-*mj*

In the present study, we created a 3-iodo-L-tyrosine-specific variant of *M. jannaschii* TyrRS, which enabled the application

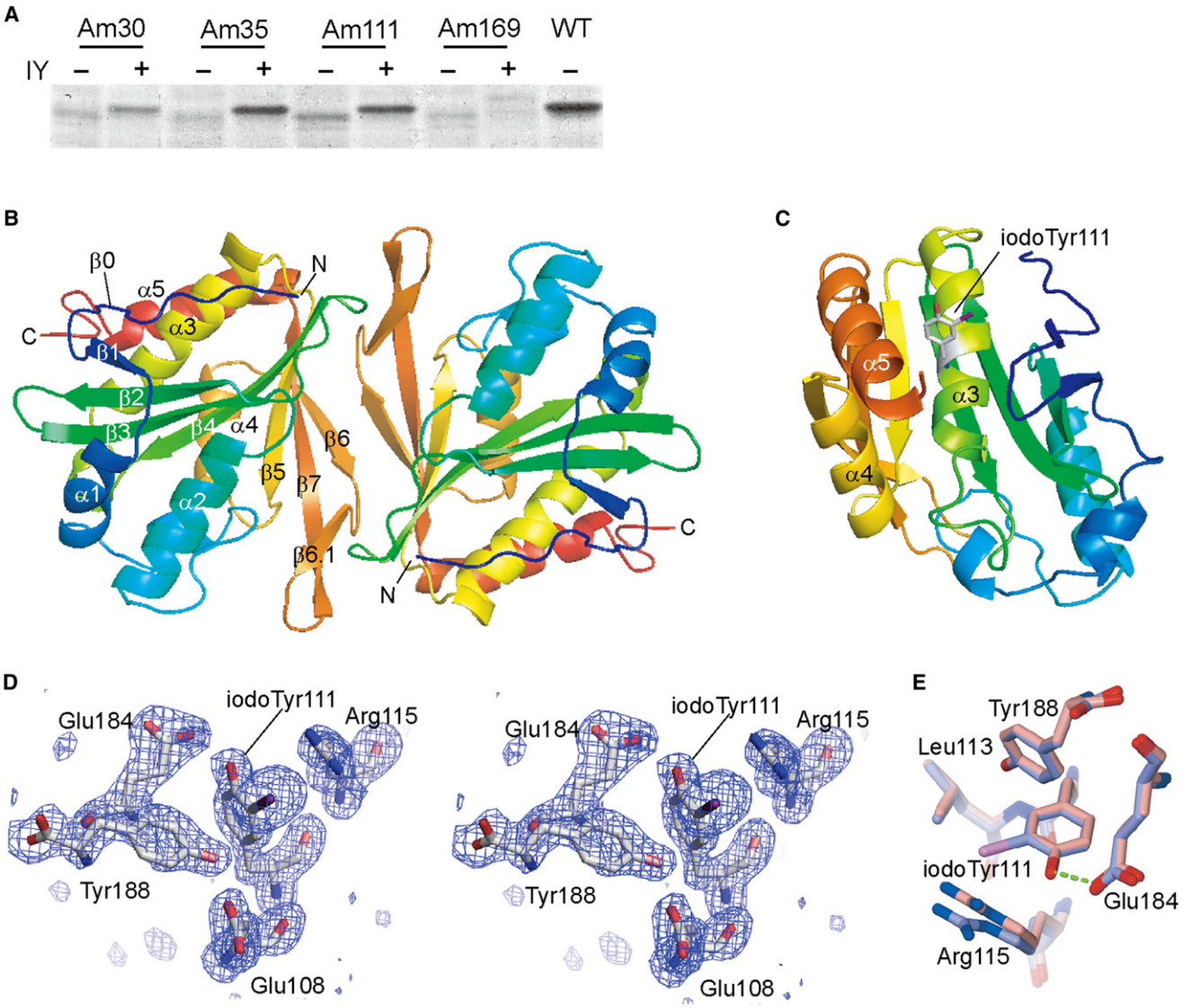

Figure 2. Structure Determination of *T. thermophilus* RimL

(A) Overproduction of RimL variants with iodotyrosine and the wild-type RimL (WT) in *E. coli* cells, in the presence and absence of 3-iodo-L-tyrosine (IY) in the growth media, was analyzed by SDS electrophoresis of the cell extracts after heat treatment.

(B) The crystal structure of the *T. thermophilus* RimL dimer is depicted by a ribbon model. Secondary structures are indicated as follows: β0, β1, and α1 (blue); α2 (cyan); β2, β3, and β4 (green); α3 and β5 (yellow), α4, β6, β6.1, and β7 (orange); and α5 (red) from the N terminus to the C terminus.

(C) The iodotyrosine at position 111 (iodoTyr111) is shown by a stick model in the monomer structure of RimL. Helices α3–α4 are indicated.

(D) Stereo view of the $|F_o - F_c|$ omit map (3.0 σ) around iodoTyr111. The iodine atom is depicted by a purple stick.

(E) Superposed partial structures of RimL(iodoTyr111) (light blue) and the wild-type RimL (pink) around position 111. The hydrogen bond is shown by a green, dotted line.

of this amino acid to SAD phasing. We previously developed a variant of *E. coli* TyrRS that prefers 3-iodo-L-tyrosine to L-tyrosine, but still appreciably recognizes L-tyrosine (Kiga et al., 2002). In the presence of competing 3-iodo-L-tyrosine, this *E. coli* variant or iodoTyrRS-*ec* hardly incorporates L-tyrosine and translates the amber codon into 3-iodo-L-tyrosine in mammalian cells (Sakamoto et al., 2002). Recently, the overall specificity of iodoTyrRS-*ec* was drastically improved by transplanting an exogenous editing domain into this variant; the resulting editing variant hardly produces tyrosyl-tRNA molecules even in the absence of 3-iodo-L-tyrosine (Oki et al., 2008).

The structural basis for the recognition of 3-iodo-L-tyrosine by iodoTyrRS-*ec*, as well as that for the recognition of L-tyrosine by *E. coli* TyrRS, was elucidated by X-ray crystallography (Kobayashi et al., 2005a, 2005b). The manner of L-tyrosine recognition is quite similar between the *M. jannaschii* and *E. coli* TyrRSs: the phenolic hydroxyl group of L-tyrosine forms two hydrogen bonds with the conserved Tyr and Asp residues at positions 32 and 158, respectively, in the archaeal TyrRS, and at positions 37 and 182, respectively, in the bacterial TyrRS (Figure S3). In spite of this similarity, iodoTyrRS-*mj* and iodoTyrRS-*ec* exhibit different 3-iodo-L-tyrosine-recognition manners: the iodine moiety

protrudes toward the opposite sides of the binding pocket. In iodoTyrRS-*mj*, His70 and Asp158 are replaced to accommodate the iodine atom, whereas Tyr32 is not mutated (Figure 1E). In iodoTyrRS-*ec*, Val replaces Tyr37 to accommodate the iodine, and Asp182 is not mutated.

These differences in the orientation of the iodine moiety of 3-iodo-L-tyrosine in the binding pocket result in the disruption of different hydrogen-bonding interactions with the hydroxyl group of the phenolic ring. The hydrogen bond involving Asp158 is missing in iodoTyrRS-*mj*, whereas the hydrogen bond involving Tyr37 is missing in iodoTyrRS-*ec* (Figure 1E). Although *E. coli* TyrRS variants with replacements of Tyr37 reportedly retain significant activity for L-tyrosine (Kiga et al., 2002), the replacement of Asp158 drastically reduced the activity of iodoTyrRS-*mj* for L-tyrosine. These observations indicate that the hydrogen bond for Asp158/182 plays a more critical role in the L-tyrosine binding than that of Tyr32/37, and that the discrimination against L-tyrosine by iodoTyrRS-*mj* is achieved by the replacement of Asp158. Meanwhile, the binding of 3-iodo-L-tyrosine to this variant largely relies on the van der Waals contacts between the iodine moiety and 5 residues: 2 mutated residues, Ala70 and Thr158; and 3 wild-type residues, Leu65, Gln109, and Met154.

The first crystal structure determined for an *M. jannaschii* TyrRS variant was that of the *O*-methyl-L-tyrosine-specific variant in the substrate-free form (Zhang et al., 2005). Since then, the crystal structures of *M. jannaschii* TyrRS variants complexed with their specific substrates, 4-bromophenylalanine, 4-acetylphenylalanine, 3-(2-naphthyl)alanine, and 4-benzoylphenylalanine (*p*Bpa), have been determined to elucidate the structural basis for the recognition of these nonnatural substrates (Turner et al., 2005, 2006; Liu, et al., 2007). These variants also lack the activity for L-tyrosine. Tyr32, Asp158, and Ile159 are replaced in all of these variants, with two or three additional replacements for each of the three variants, other than the *p*Bpa-specific variant (*Mj*pBpaRS). The variants other than *Mj*pBpaRS contain the Asp158Pro or Asp158Gly mutation, which causes a large structural rearrangement involving the shift of the main chain atoms at the binding pocket, and thus creates space for the bulky substituents on their nonnatural substrates.

However, *Mj*pBpaRS with Tyr32Gly, Asp158Thr, and Ile159Ser has a moderately reshaped binding pocket, with no changes in the position of the main chain atoms, which is similar to the case of iodoTyrRS-*mj*, with Asp158Thr and Ile159Ser in common. All three of the replacements in *Mj*pBpaRS mainly contribute to creating space for the bulky benzoyl group, which extends in the opposite direction from the iodine atom in iodoTyrRS-*mj*. In the absence of Tyr32, Ser159 of *Mj*pBpaRS does not form the expanded network of hydrogen bonds, as found in iodoTyrRS-*mj*. The difference between Tyr32Gly and His70Ala confers the distinct substrate specificity between these two variants, which both have a moderately reshaped binding pocket.

Comparison between the Crystal Structures of *T. thermophilus* RimL and Two Other Bacterial Ribosomal Protein *N*-Acetyltransferases

The crystal structure of *T. thermophilus* RimL exhibits a GCN5-related *N*-acetyltransferase fold (Clements et al., 1999; Rojas et al., 1999; Angus-Hill et al., 1999) (Figure 2B) and resembles the crystal structures of the YdaF protein from *Bacillus subtilis* (Brunzelle et al., 2004) and the ribosomal protein *N*-acetyltransferase, the *rimL* gene product, from *Salmonella typhimurium* (Vetting et al., 2005) (Figure 3A). The crystal structure of *S. typhimurium* RimL includes a bound coenzyme-A molecule. YdaF is a homolog of *S. typhimurium* RimL, and we refer to it as *B. subtilis* RimL here. *T. thermophilus* RimL exhibits a 32% amino acid identity with *B. subtilis* RimL, but no significant similarity with *S. typhimurium* RimL. A multiple alignment of the amino acid sequences (Figure S4) revealed that a high sequence similarity exists among these enzymes in the region from β3 to β7. This β3–β7 region contains a CoA-binding site of *S. typhimurium* RimL and corresponds to the region encompassing the CoA-binding motifs, A and B, of GCN5-related *N*-acetyltransferases.

The *S. typhimurium* and *B. subtilis* RimL molecules also reportedly exist as homodimers in solution (Brunzelle et al., 2004; Vetting et al., 2005). The dimerization of *T. thermophilus* RimL, as well as that of these enzymes, involves the β6 strands from each monomer, which are paired with each other in an antiparallel manner (Figure 2B). A cleft is formed at the dimer interface for all of these RimLs, and the β6 and β7 strands form the floor of the cleft. In a surface potential representation, the dimer of *S. typhimurium* RimL has a positively charged patch accommodating the phosphate moiety of CoA in each monomer, and the corresponding basic patches also exist in the other two enzymes (Figure 3B, CoA side).

The pantetheine arm of the acetyl-CoA bound to *S. typhimurium* RimL extends to the opposite side of the enzyme from the basic patch, to donate the acetyl group to the substrate, as in the reported coenzyme-bound structures of GCN5-related *N*-acetyltransferases. Thus, the cleft formed along the dimer interface and located on the opposite side of the basic patches (Figure 3B, cleft side) probably serves as a substrate-binding site for *S. typhimurium* RimL (Vetting et al., 2005). RimL acetylates the N-terminal amino group of ribosomal protein L12, to convert L12 to L7 (Tanaka et al., 1989). It has been proposed that the cleft of the *S. typhimurium* RimL dimer binds two sets of the N-terminal α_1 and α_2 helices from the L12 dimer, and that the lining of the cleft with a mixture of basic, acidic, and aliphatic residues may reflect the mixed nature of the N-terminal helices of L12 from *S. typhimurium* (Vetting et al., 2005) (Figure 3C). The highly acidic nature of the cleft of *B. subtilis* RimL appears to fit the positively charged N-terminal region of *B. subtilis* L12, whereas *T. thermophilus* RimL, with a cleft containing mixed residues, may bind to the N terminus of *T. thermophilus* L12 with an accordingly mixed nature (Figure 3C). The cleft of *T. thermophilus* RimL is narrower than those of the other two RimL molecules, because the loop after the α2 helix of *T. thermophilus* RimL bulges out toward the center of the cleft (Figures 3A and 3B). This loop may assume a more compact form to widen the cleft when RimL binds to the N-terminal helices of L12.

Applicability of 3-Iodo-L-Tyrosine to the Determination of Protein Structures

We successfully determined the crystal structure of an iodotyrosine-containing variant of *T. thermophilus* RimL, RimL(iodoTyr111), by SAD experiments with an in-house X-ray generator.

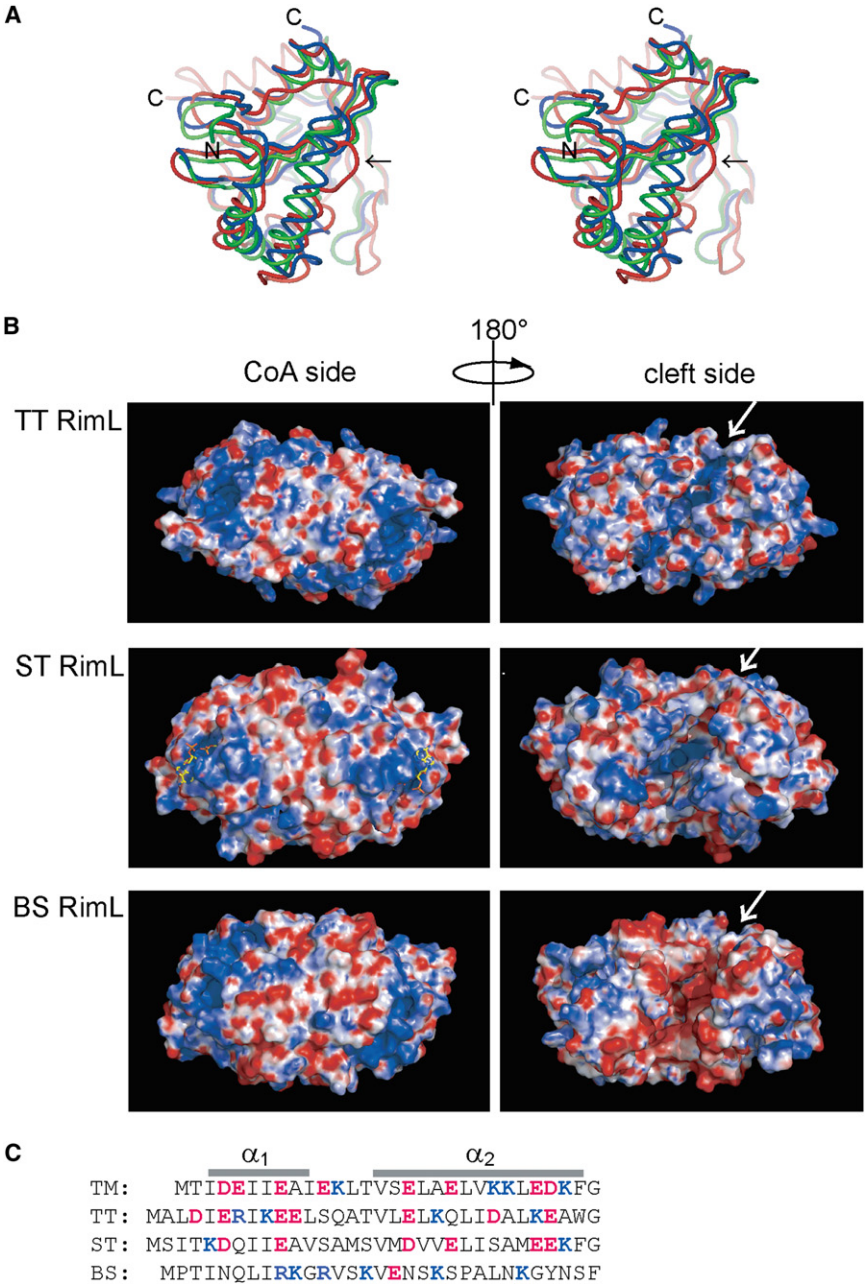

Figure 3. Comparison between the Three Bacterial RimL Molecules

(A) A stereo view of the superposed structures of the RimL molecules from *T. thermophilus* (red), *S. typhimurium* (blue), and *B. subtilis* (green) are shown. The N and C termini are marked. The bulging loop after the *T. thermophilus* α2 helix is indicated by the arrow.

(B) Surface potential representations of the dimers of *T. thermophilus* RimL (TT RimL), *S. typhimurium* RimL (ST RimL), and *B. subtilis* RimL (BS RimL) are shown. The view of the "cleft side" is a 180° rotation from that of the "CoA side." Red, blue, and white represent acidic, basic, and neutral, respectively. The two CoA molecules bound to ST RimL are represented by sticks in the view of the CoA side. The clefts are indicated by white arrows. The electrostatic potential was calculated by using the GRASP program (Nicholls et al., 1991).

(C) Alignment of the N-terminal amino acid sequences of the L12 proteins from TM (*Thermotoga maritima*), TT (*T. thermophilus*), ST (*S. typhimurium*), and BS (*B. subtilis*). The secondary structures indicated above the alignment correspond to those of *T. maritima* L12. Acidic and basic residues are denoted by red and blue letters, respectively.

A comparison with the native structure of RimL revealed no significant structural distortion caused by the iodotyrosine incorporation. Twinned crystals were obtained from another variant, RimL(iodoTyr35), and its tertiary structure exhibited a difference limited to the structure of the loop with iodoTyr35. One of the five tyrosines in RimL is located near the C terminus, and it was not tested for replacement with iodotyrosine. In a situation in which the C-terminal tagging with a peptide sequence is allowed for detecting suppression products, there is no restriction, in principle, on the position of the tyrosine to be replaced with the nonnatural amino acid.

The SAD phasing with this amino acid provides the following advantages. First, it is useful for proteins with few methionines, for which the phasing strategy with selenomethionine is not typically employed. Second, *E. coli* cells producing iodotyrosine-containing proteins can be cultured in rich media, promising a large yield of the alloprotein per unit volume of cell culture. Finally, the CuKα and CrKα wavelengths for SAD phasing are available on in-house X-ray generators. These advantages also hold with the use of iodophenylalanine.

In the native structure of *T. thermophilus* RimL, the solvent-exposed areas of Tyr169, Tyr35, Tyr111, and Tyr30 were calculated as 0.3, 2.3, 9.9, and 69 Å^2, respectively. The inability to express RimL(iodoTyr169) was probably related to the least exposure of Tyr169, and the bulky iodine atom at this position may cause fatal steric hindrance. Therefore, without any prior knowledge of the tertiary structure, the replacement of Tyr is probably preferable to that of Phe, because Tyr is usually more solvent exposed (Bordo and Argos, 1991). The unsuccessful crystallization of RimL (iodoTyr30) was probably due to the aggregated state of this variant in solution. Biophysical analyses are helpful to select promising variants among those that can be expressed, for structure determination. The applicability of 3-iodo-L-tyrosine is enhanced by the fact that this amino acid has been site specifically incorporated into proteins in mammalian cells by using iodoTyrRS-*ec*, and the mammalian system is also applicable to the preparation of iodinated proteins for crystallography.

EXPERIMENTAL PROCEDURES

Isolation and Characterization of IodoTyrRS-*mj*

The genes encoding *M. jannaschii* TyrRS variants were cloned after the *E. coli tyrS* promoter in the vector pACYC184, together with the gene for an *M. jannaschii* suppressor tRNA (Wang et al., 2001), to create the pMjYSmu-MJR1 plasmids. The tRNA gene was transcribed from the *E. coli lpp* promoter to the *rrnC* terminator. Random mutagenesis at a defined codon was performed by polymerase chain reaction (PCR) with a mutagenic primer to replace the codon with the NNK sequence, where N is any of the four nucleotides, and K is G or T. The gene for CAT, with an amber codon in place of Thr10, was cloned into pBR322 to create the plasmid pBR322Cm(Am). This plasmid was introduced into a suppressor-tRNA-free *E. coli* strain, TOP10 (Invitrogen), together with the pMjYSmu-MJR1 plasmids. The transformed cells were grown on an LB agarose plate containing Cm (50 or 200 μg/ml) and 3-iodo-L-tyrosine (0.1 mg/ml), which was purchased from Sigma-Aldrich. The formed colonies were replicated on an LB plate containing Cm (50 μg/ml), but not 3-iodo-L-tyrosine.

The iodoTyrRS-*mj* with a His tag at the C terminus was expressed from pET26b (Novagen) in the *E. coli* BL21 Star(DE3) strain (Invitrogen) to be purified for in vitro aminoacylation. The preparation of *M. jannaschii* TyrRS and $tRNA^{Tyr}$ was previously described (Kobayashi et al., 2003). The cells were grown in LB medium at 37°C. Isopropyl-β-D-thiogalactopyranoside (IPTG) (1 mM) was added to induce the expression of iodoTyrRS-*mj*, when the optical density of the cell culture reached 0.4 at 600 nm, and the cells were grown for an additional 3 hr. The products were purified by chromatography on His-trap HP and Resource Q columns, both purchased from GE Healthcare. The aminoacylation of *M. jannaschii* $tRNA^{Tyr}$ (5 μM) was performed at 37°C for 2 hr, in 20 μl of HEPES-Na buffer (pH 7.5) containing $MgCl_2$ (15 mM), DTT (1 mM), ATP (10 mM), bovine serum albumin (50 μg/ml), and L-tyrosine or 3-iodo-L-tyrosine (0.1 mM). *M. jannaschii* TyrRS (5 nM) or iodoTyrRS-*mj* (10 μM) was added to this reaction. A 5 μl aliquot of the reaction was analyzed by electrophoresis on a denaturing acidic polyacrylamide gel as described (Varshney et al., 1991).

The *gst* gene from *Schistosoma japonicum* had the additional sequence 5′-MASMTGGQQMGRDPGANSGVTKNSY-3′ in place of the N-terminal Met, where the underlined Tyr was replaced with an amber codon to create the *gst*(Am25) gene. The *gst* and *gst*(Am25) genes were cloned between the BamHI and XhoI sites of the vector pET21b (Novagen) to create pET21GST and pET21GST(Am25), respectively. The BL21(DE3) strain was transformed with pET21GST or with both pET21GST(Am25) and the pMjYSmu-MJR1 plasmid carrying the iodoTyrRS-*mj* gene (piodoTyrRS-MJR1). The transformed cells were grown in LB medium with 3-iodo-L-tyrosine (0.1 mg/ml), and the induction with IPTG (1 mM) was performed at an OD_{600} of 0.4, followed by a further incubation for 10 hr. The products were purified by using the GST purification module (GE Healthcare). The mass spectrometric analysis of the peptides from the GST products was commercially performed by Shimadzu Biotech (Tsukuba, Japan).

Crystallization, Data Collection, and Structure Determination for iodoTyrRS-*mj*

Crystallization of iodoTyrRS-*mj* complexed with 3-iodo-L-tyrosine was performed by the hanging-drop vapor-diffusion method at 20°C. A 1 μl aliquot of the protein sample was mixed with 1 μl reservoir solution (100 mM Tris-Cl [pH 8.5] buffer containing 24%–28% PEG 300, 5%–8% PEG 8,000, and 10% glycerol). Square rod-like crystals appeared within 2 days and reached maximal dimensions (0.15 × 0.15 × 1.0 mm^3) in 2 weeks. The crystals were soaked in a cryoprotectant solution, containing all of the components of the reservoir solution and 2 mM 3-iodo-L-tyrosine, and were flash cooled at 100 K. A native data set at 1.7 Å resolution was collected at the beamline AR-NW12A, Photon Factory (Tsukuba, Japan), and was processed with the DENZO and SCALEPACK programs (Otwinowski and Minor, 1997). The structure of the iodoTyrRS-*mj*•3-iodo-L-tyrosine complex was solved by molecular replacement, by using the program REFMAC5 (CCP4, 1994). The *M. jannaschii* TyrRS variant specific for *p*-bromophenylalanine (Protein Data Bank accession code 2AG6) was used as a search model. The 3-iodo-L-tyrosine model was generated with the Dundee PRODRG server (http://davapc1.bioch.dundee.ac.uk/prodrg/), and then the model of the iodoTyrRS-*mj*•3-iodo-L-tyrosine complex was generated with CNS (Brunger et al., 1998). The final model of the complex was built manually, by using COOT (Emsley and Cowtan, 2004). Refinement of the complex structure was carried out by using CNS; rigid-body refinement and several rounds of simulated annealing refinement (with a starting temperature of 2500 K) and individual B factor refinement were performed. A random 10% of the starting data was set aside for cross-validation. After the majority of the model was built, the water molecules were picked automatically, as implemented in CNS, and several rounds of refinement were executed. The stereochemical quality of the final models was assessed by PROCHECK (Laskowski et al., 1993). The water molecules were then selected manually, and the refinement converged to a final R factor of 19.3%, with an R_{free} of 22.0% (resolution range of 41.7–1.7 Å).

Preparation of RimL Variants

The *rimL* gene (the *TTHA1799* gene from *T. thermophilus* HB8) and its amber mutants were cloned in pET vectors for overproduction in the strain BL21(DE3). Amber mutations were generated by PCR with appropriate mutagenic primers, and, at this step, the C-terminal Pro194 codon was removed from the variant genes. Neither the RimL protein nor its variants were terminally tagged. For preparing the variants, the cells were transformed with both the pET plasmids expressing the *rimL* amber mutants and the piodoTyrRS-MJR1 plasmid. The cells were grown in LB medium with 3-iodo-L-tyrosine (0.1 mg/ml), and the induction with IPTG (1 mM) was performed at an OD_{600} of 0.4, followed by a further incubation for 10 hr. The expression of amber mutants was analyzed by SDS-PAGE, after heat treatment of the cell extracts at 70°C for 30 min. RimL and its variants were purified from the heat-treated extracts by successive chromatography steps on columns of HiTrap Butyl, Resource S, Resource Q, and HiLoad 16/60 Superdex75, all purchased from GE Healthcare.

Crystallization, Data Collection, and Structure Determination for RimL

Crystallization of *T. thermophilus* RimL and its variants was performed by the hanging-drop vapor-diffusion method at 20°C. A 1 μl aliquot of the protein sample was mixed with 1 μl reservoir solution, which was 0.1 M Bis-Tris buffer (pH 5.5) containing 28% PEG 3,350 and 0.15 M ammonium acetate for RimL (iodoTyr111), 0.1 M Bis-Tris buffer (pH 6.5) containing 25% PEG 3,350 and 0.2 M $MgCl_2$ for RimL(iodoTyr35), or 0.1 M Bis-Tris buffer (pH 5.5) containing 1 M ammonium sulfate and 15% glycerol for the native protein. Prismatic crystals were grown to approximate dimensions of 0.20 × 0.20 × 0.15 mm^3 within a week. Two sets of X-ray data were collected with in-house CuKα and CrKα radiation (1.5418 Å and 2.2908 Å, respectively), by using R-AXIS IV^{2+} imaging-plate detectors mounted on FR-E superbrilliant X-ray generators (Rigaku/MSC), with a Cu or Cr rotating-anode target, under cryogenic conditions. Paratone N and 30% glycerol were used for the crystals of RimL variants and that of the native protein, respectively, as cryoprotectants. The diffraction data were processed with the HKL2000 program package (Otwinowski and Minor, 1997). The initial phase for the RimL(iodoTyr111) structure was solved by the single-wavelength anomalous dispersion method. The Cr-SAD and Cu-SAD data at 2.15 Å and 1.77 Å resolution, respectively, were processed with SOLVE (Terwilliger, 2003). Density modification and phase refinement were performed with RESOLVE, which yielded a clearly interpretable electron density map. The structure models of RimL(iodoTyr111) were built with O (Jones et al., 1991) and refined with CNS. The crystal structures of the native protein and RimL(iodoTyr35) were solved by molecular replacement, by using MolRep in CCP4i (Potterton et al., 2003), with the RimL(iodoTyr111) structure as a search model. For the refinement of the structure of RimL(iodoTyr35), the refinement protocols for twinned crystal in CNS were used with a twin fraction 0.443. The stereochemical quality of the final models was assessed by PROCHECK.

Structure Rendering

The structural images were generated by using CUEMOL (http://cuemol.sourceforge.jp/ja/) and were rendered by using POV-RAY (http://www.povray.org/).

ACCESSION NUMBERS

The structure coordinates have been deposited in the Protein Data Bank with the accession codes 2Z0Z (native RimL), 2Z10 (RimL[iodoTyr111]-CuKα),

2Z11 (RimL[iodoTyr111]-CrKα), 2ZXV (RimL[iodoTyr35]-CuKα), and 2ZP1 (iodoTyrRS-*mj*•3-iodo-L-tyrosine).

SUPPLEMENTAL DATA

Supplemental Data include four figures and can be found with this article online at http://www.cell.com/structure/supplemental/S0969-2126(09)00071-9.

ACKNOWLEDGMENTS

We thank N. Obayashi and K. Katsura and T. Terada for the purification of RimL variant, as well as A. Ishii and T. Nakayama for clerical assistance. This work was supported by the Targeted Proteins Research Program (TPRP), and by the RIKEN Structural Genomics/Proteomics Initiative (RSGI) in the National Project on Protein Structural and Functional Analyses, from the Ministry of Education, Culture, Sports, Science and Technology (MEXT) of Japan, and it was supported in part by a Grant-in-Aid for Scientific Research B (19380195) from MEXT. T.K. was supported in part by the Special Postdoctoral Researchers Program at RIKEN.

Received: October 21, 2008
Revised: January 15, 2009
Accepted: January 15, 2009
Published: March 10, 2009

REFERENCES

Angus-Hill, M.L., Duinall, R.N., Tafrov, S.T., Sternglanz, R., and Ramakrishnan, V. (1999). Crystal structure of the histone acetyltransferase Hpa2: a tetrameric member of the Gcn5-related *N*-actyltransferase superfamily. J. Mol. Biol. *294*, 1311–1325.

Bain, J.D., Glabe, C.G., Dix, T.A., Chamberlin, A.R., and Diala, E.S. (1989). Biosynthetic site-specific incorporation of a non-natural amino acid into a polypeptide. J. Am. Chem. Soc. *111*, 8013–8014.

Bordo, D., and Argos, P. (1991). Suggestions for "safe" residue substitutions in site-directed mutagenesis. J. Mol. Biol. *217*, 721–729.

Brunzelle, J.S., Wu, R., Korolev, S.V., Collart, F.R., Joachimiak, A., and Anderson, W.F. (2004). Crystal structure of *Bacillus subtilis* YdaF protein: a putative ribosomal *N*-acetyltransferase. Proteins *57*, 850–853.

Brunger, A.T., Adams, P.D., Clore, G.M., DeLano, W.L., Gros, P., Grosse-Kunstleve, R.W., Jiang, J.S., Kuszewski, J., Nilges, M., Pannu, N.S., et al. (1998). Crystallography and NMR system: a new software suite for macromolecular structure determination. Acta Crystallogr. D Biol. Crystallogr. *54*, 905–921.

Chin, J.W., Cropp, T.A., Anderson, J.C., Mukherji, M., Zhang, Z., and Schultz, P.G. (2003). An expanded eukaryotic genetic code. Science *301*, 964–967.

Clements, A., Rojas, J.R., Trievel, R.C., Wang, L., Berger, S.L., and Marmorstein, R. (1999). Crystal structure of the histone acetyltransferase domain of the human PCAF transcriptional regulator bound to coenzyme A. EMBO J. *18*, 3521–3532.

Collaborative Computational Project, Number 4 (CCP4). (1994). The CCP4 suite: programs for protein crystallography. Acta Crystallogr. D Biol. Crystallogr. *50*, 760–763.

Cornish, V.W., Mendel, D., and Schultz, P.G. (1995). Probing protein structure and function with an expanded genetic code. Angew. Chem. Int. Ed. Engl. *34*, 621–633.

Dauter, Z., Dauter, M., Dodson, E., and Jolly, S.A.D. (2002). Jolly SAD. Acta Crystallogr. D Biol. Crystallogr. *58*, 494–506.

Emsley, P., and Cowtan, K. (2004). Coot: model-building tools for molecular graphics. Acta Crystallogr. D Biol. Crystallogr. *60*, 2126–2132.

Hendrickson, W.A. (1991). Determination of macromolecular structures from anomalous diffraction of synchrotron radiation. Science *254*, 51–58.

Henne, A., Brüggemann, H., Raasch, C., Wiezer, A., Hartsch, T., Liesegang, H., Johann, A., Lienard, T., Gohl, O., Martinez-Arias, R., et al. (2004). The genome sequence of the extreme thermophile *Thermus thermophilus*. Nat. Biotechnol. *22*, 547–553.

Hohsaka, T., Ashizuka, Y., Taira, H., Murakami, H., and Sisido, M. (2001). Incorporation of nonnatural amino acids into proteins by using various four-base codons in an *Escherichia coli in vitro* translation system. Biochemistry *40*, 11060–11064.

Jones, T.A., Zou, J.Y., Cowan, S.W., and Kjeldgaard, M. (1991). Improved methods for building protein models in electron density maps and the location of errors in these models. Acta Crystallogr. A *47*, 110–119.

Laskowski, R.A., MacArthur, M.W., Moss, D.S., and Thornton, J.M. (1993). PROCHECK: a program to check the stereochemical quality of protein structures. J. Appl. Crystallogr. *26*, 283–291.

Li, Y., Bahti, P., Shaw, N., Song, G., Chen, S., Zhang, X., Zhang, M., Cheng, C., Tin, J., Zhu, J.-Y., et al. (2008). Crystal structure of a novel non-Pfam protein AF1514 from *Archeoglobus fulgidus* DSM 4304 solved by S-SAD using a Cr X-ray source. Proteins *71*, 2109–2113.

Liu, W., Alfonta, L., Mack, A.V., and Schultz, P.G. (2007). Structural basis for the recognition of *para*-benzoyl-L-phenylalanine by evolved aminoacyl-tRNA synthetases. Angew. Chem. Int. Ed. Engl. *46*, 6073–6075.

Kiga, D., Sakamoto, K., Kodama, K., Kigawa, T., Matsuda, T., Yabuki, T., Shirouzu, M., Harada, Y., Nakayama, H., Takio, K., et al. (2002). An engineered *Escherichia coli* tyrosyl-tRNA synthetase for site-specific incorporation of an unnatural amino acid into proteins in eukaryotic translation and its application in a wheat germ cell-free system. Proc. Natl. Acad. Sci. USA *99*, 9715–9723.

Kobayashi, T., Nureki, O., Ishitani, R., Yaremchuk, A., Tukalo, M., Cusack, S., Sakamoto, K., and Yokoyama, S. (2003). Structural basis for orthogonal tRNA specificities of tyrosyl-tRNA synthetases for genetic code expansion. Nat. Struct. Biol. *10*, 425–432.

Kobayashi, T., Sakamoto, K., Takimura, T., Sekine, R., Vincent, K., Kamata, K., Nishimura, S., and Yokoyama, S. (2005a). Structural basis of nonnatural amino acid recognition by an engineered aminoacyl-tRNA synthetase for genetic code expansion. Proc. Natl. Acad. Sci. USA *102*, 1366–1371.

Kobayashi, T., Takimura, T., Sekine, R., Vincent, K., Kamata, K., Sakamoto, K., Nishimura, S., and Yokoyama, S. (2005b). Structural snapshots of the KMSKS loop rearrangement for amino acid activation by bacterial tyrosyl-tRNA synthetase. J. Mol. Biol. *346*, 105–117.

Nicholls, A., Sharp, K.A., and Honig, B. (1991). Protein folding and association: insights from the interfacial and thermodynamic properties of hydrocarbons. Proteins *11*, 281–296.

Noren, C.J., Anthony-Cahill, S.J., Griffith, M.C., and Schultz, P.G. (1989). A general method for site-specific incorporation of unnatural amino acids into proteins. Science *244*, 182–188.

Oki, K., Sakamoto, K., Kobayashi, T., Sasaki, H.M., and Yokoyama, S. (2008). Transplantation of a tyrosine editing domain into a tyrosyl-tRNA synthetase variant enhances its specificity for a tyrosine analog. Proc. Natl. Acad. Sci. USA *105*, 13298–13303.

Otwinowski, Z., and Minor, W. (1997). Processing of X-ray diffraction data collected in oscillation mode. Methods Enzymol. *276*, 307–326.

Potterton, E., Briggs, P., Turkenburg, M., and Dodson, E. (2003). A graphical user interface to the CCP4 program suite. Acta Crystallogr. D Biol. Crystallogr. *59*, 1131–1137.

Rojas, J.R., Trievel, R.C., Zhou, J., Mo, Y., Li, X., Berger, S.L., Allis, D., and Marmorstein, R. (1999). Structure of Tetrahymena GCN5 bound to coenzyme A and a histone H3 peptide. Nature *401*, 93–98.

Sakamoto, K., Hayashi, A., Sakamoto, A., Kiga, D., Nakayama, H., Soma, A., Kobayashi, T., Kitabatake, M., Takio, T., Saito, K., et al. (2002). Site-specific incorporation of an unnatural amino acid into proteins in mammalian cells. Nucleic Acids Res. *30*, 4692–4699.

Tanaka, S., Matsushita, Y., Yoshikawa, A., and Isono, K. (1989). Cloning and molecular characterization of the gene *rimL* which encodes an enzyme acetylating ribosomal protein L12 of *Escherichia coli* K12. Mol. Gen. Genet. *217*, 289–293.

Teeter, M.M., and Hendrickson, W.A. (1979). Highly ordered crystals of the plant seed protein crambin. J. Mol. Biol. *127*, 219–223.

Terwilliger, T.C. (2003). SOLVE and RESOLVE: automated structure solution and density modification. Methods Enzymol. *374*, 22–37.

Turner, J.M., Graziano, J., Spraggon, G., and Shultz, P.G. (2005). Structural characterization of a p-acetylphenylalanyl aminoacyl-tRNA synthetase. J. Am. Chem. Soc. *127*, 14976–14977.

Turner, J.M., Graziano, J., Spraggon, G., and Shultz, P.G. (2006). Structural plasticity of an aminoacyl-tRNA synthetase active site. Proc. Natl. Acad. Sci. USA *103*, 6483–6488.

Varshney, U., Lee, C.-P., and RajBhandary, U.L. (1991). Direct analysis of aminoacylation levels of tRNAs *in vivo*. J. Biol. Chem. *266*, 24712–24718.

Vetting, M.W., de Carvalho, L.P.S., Roderick, S.L., and Blanchard, J.S. (2005). A novel dimeric structure of the RimL N^{α}-acetyltransferase from *Salmonella typhimurium*. J. Biol. Chem. *280*, 22108–22114.

Wang, L., Brock, A., Herberich, B., and Schultz, P.G. (2001). Expanding the genetic code of *Escherichia coli*. Science *292*, 498–500.

Xie, J., Wang, L., Wu, N., Brock, A., Spraggon, G., and Schultz, P.G. (2004). The site-specific incorporation of *p*-iodo-L-phenylalanine into proteins for structure determination. Nat. Biotechnol. *22*, 1297–1301.

Ye, S., Köhrer, C., Huber, T., Kazmi, M., Sachdev, P., Yan, E.C.Y., Bhagat, A., RajBhandary, U.L., and Sakmar, T.P. (2008). Site-specitic incorporation of keto amino acids into functional G protein-coupled receptors using unnatural amino acid mutagenesis. J. Biol. Chem. *283*, 1525–1533.

Zhang, Y., Wang, L., Schultz, P.G., and Wilson, I.A. (2005). Crystal structures of apo wild-type *M. jannaschii* tyrosyl-tRNA synthetase (TyrRS) and an engineered TyrRS specific for *O*-methyl-L-tyrosine. Protein Sci. *14*, 1340–1349.

